Forced synchronization of periodic and aperiodic thermoacoustic oscillations: lock-in, bifurcations and open-loop control

Karthik Kashinath[1],[†], Larry K. B. Li[2] and Matthew P. Juniper[3]

[1]Lawrence Berkeley National Laboratory, Climate Science Department – Earth and Environmental Sciences Area, 1 Cyclotron Road, Berkeley, CA 94720, USA

[2]Department of Mechanical and Aerospace Engineering, The Hong Kong University of Science and Technology, Clear Water Bay, Hong Kong

[3]Department of Engineering, University of Cambridge, Trumpington Street, Cambridge CB2 1PZ, UK

Synchronization is a universal concept in nonlinear science but has received little attention in thermoacoustics. In this numerical study, we take a dynamical systems approach to investigating the influence of harmonic acoustic forcing on three different types of self-excited thermoacoustic oscillations: periodic, quasi-periodic and chaotic. When the periodic system is forced, we find that: (i) at low forcing amplitudes, it responds at both the forcing frequency and the natural (self-excited) frequency, as well as at their linear combinations, indicating quasi-periodicity; (ii) above a critical forcing amplitude, the system locks in to the forcing; (iii) the bifurcations leading up to lock-in and the critical forcing amplitude required for lock-in depend on the proximity of the forcing frequency to the natural frequency; (iv) the response amplitude at lock-in may be larger or smaller than that of the unforced system and the system can exhibit hysteresis and the jump phenomenon owing to a cusp catastrophe; and (v) at forcing amplitudes above lock-in, the oscillations can become unstable and transition to chaos, or switch between different stable attractors depending on the forcing amplitude. When the quasi-periodic system is forced at a frequency equal to one of the two characteristic frequencies of the torus attractor, we find that lock-in occurs via a saddle-node bifurcation with frequency pulling. When the chaotic system is forced at a frequency close to the dominant frequency of its strange attractor, we find that it is possible to destroy chaos and establish stable periodic oscillations. These results show that the open-loop application of harmonic acoustic forcing can be an effective strategy for controlling periodic or aperiodic thermoacoustic oscillations. In some cases, we find that such forcing can reduce the response amplitude by up to 90 %, making it a viable way to weaken thermoacoustic oscillations.

Key words: bifurcation, chaos, noise control

† Email address for correspondence: karthikkashinath@gmail.com

1. Introduction

A self-excited nonlinear system oscillating periodically at one frequency can be forced to oscillate at a different frequency when subjected to external forcing (Pikovsky, Rosenblum & Kurths 2003). This process is known as forced synchronization. It has been studied in various natural and human-made systems, including pendulum clocks (Huygens 1673), chemical reactions (Petrov, Ouyang & Swinney 1997), circadian rhythms (Rompala, Rand & Howland 2007), neurons (Hopfield 1994) and organ pipes (Abel, Ahnert & Bergweiler 2009). It has also been modelled accurately with universal low-dimensional oscillators such as the forced van der Pol (1927) oscillator. The use of external forcing to control or suppress self-excited oscillations has been attracting growing interest because of its applicability to fields as wide ranging as hydrodynamics, electromagnetics, neuronics and thermoacoustics (Hovel 2010).

In thermoacoustic systems, such as gas turbines used for power generation and aircraft propulsion, self-excited pressure oscillations can arise from the coupling between unsteady heat release and acoustics, leading to increased noise and pollutant emissions (Lieuwen & Yang 2005). Experiments (Kabiraj & Sujith 2012; Kabiraj *et al.* 2012*a*; Kabiraj, Sujith & Wahi 2012*b*) and low-order simulations (Kashinath, Waugh & Juniper 2014) have shown that even simple thermoacoustic systems (e.g. a laminar premixed flame in a duct) can exhibit rich nonlinear behaviour. For example, they can undergo multiple bifurcations as a control parameter is varied, producing not just period-1 oscillations but also quasi-periodic, intermittent, frequency-locked, chaotic or period-k oscillations. Experiments on more complex thermoacoustic systems have revealed similarly elaborate dynamics (Gotoda *et al.* 2011, 2012). However, the effect of external harmonic forcing on such systems, particularly those that oscillate quasi-periodically or chaotically, has not been studied before.

Nevertheless, for thermoacoustic oscillations that are periodic, various control methods have been demonstrated (Dowling & Morgans 2005). In combusting systems, harmonic forcing of the fuel flow rate at the same frequency as a periodic self-excited mode, but out of phase with it, has been implemented for feedback control (Lubarsky *et al.* 2003). Recently, more sophisticated strategies have been proposed using model-based control (Annaswamy 2006) and adaptive feedback control (Illingworth & Morgans 2010). However, although feedback control works well in simple thermoacoustic systems, it is challenging in industrial systems because the sensors and actuators have to withstand harsh environments. It is also unacceptably risky in some applications, such as aircraft.

For those reasons, open-loop control is preferred. In laboratory experiments, Bellows, Hreiz & Lieuwen (2008) and Balusamy *et al.* (2015) investigated the effectiveness of open-loop harmonic acoustic forcing as a means of weakening self-excited thermoacoustic oscillations in lean-premixed swirl-stabilized turbulent combustors. They found that: (i) the oscillations can be synchronized by strong external forcing; (ii) the overall acoustic power can be reduced by the forcing, with maximum reductions of up to 90 % near lock-in; but that (iii) weak forcing ($u'/U_0 < 10\%$) has no appreciable effect on the amplitude or frequency content of the oscillations. This last finding could be due to two reasons: (i) the high noise levels in those large-scale turbulent combustors, and (ii) the use of forcing frequencies that were far away from the natural frequencies of the system.

Bellows *et al.* (2008) and Balusamy *et al.* (2015) also mentioned that the system response is complicated by hydrodynamic instabilities and their interactions with the acoustic forcing. Recent experiments have shown that forced self-excited

hydrodynamic systems can exhibit rich nonlinear behaviour near lock-in, including multiple bifurcations, quasi-periodicity and frequency pulling (Li & Juniper 2013*a*,*b*,*c*). These dynamics have not been studied in combustion-driven thermoacoustic systems, but need to be understood and accounted for during initial design or when developing control strategies.

Intrigued by the rich nonlinear dynamics of forced synchronization and motivated by the success of open-loop forcing in weakening self-excited oscillations, we explore the influence of external (open-loop) acoustic forcing on a simple thermoacoustic system (a laminar premixed flame in a duct) that oscillates periodically, quasi-periodically or chaotically. We use the coupled dynamical model described in our previous study (Kashinath *et al.* 2014) because: (i) it can accurately capture the dynamics and bifurcations seen in experiments; (ii) it has only 5000 degrees of freedom, which is significantly fewer than a comparable high-fidelity computational fluid dynamics simulation; and (iii) it is a relatively simple model consisting of a few coupled nonlinear oscillators, for which low-dimensional chaotic analogues exist in the synchronization literature (Pikovsky *et al.* 2003). Dynamical systems theory has been used extensively to study synchronization in nonlinear systems and provides a suitable framework within which to investigate this problem in thermoacoustics.

The aims of this study are as follows: (i) to investigate the influence of open-loop harmonic acoustic forcing on three different types of self-excited thermoacoustic oscillations, namely periodic, quasi-periodic and chaotic; (ii) to characterize the synchronization dynamics leading up to and beyond lock-in, including identifying the bifurcations that cause lock-in and their positions on the primary (1 : 1) Arnold tongue; and (iii) to explore the feasibility of using open-loop forcing to weaken aperiodic thermoacoustic oscillations.

In §2 we introduce the low-order coupled dynamical model. In §3 we present the dynamics of the unforced self-excited system. In §4 we discuss the influence of forcing above and below the natural (self-excited) frequency of period-1 oscillations, at various forcing amplitudes. In §4.4 we construct a lock-in map centred on the 1 : 1 Arnold tongue, examine its bifurcations and asymmetries, and discuss the implications for controlling period-1 oscillations in thermoacoustic systems. In §5 we discuss the influence of harmonic forcing on quasi-periodic and chaotic oscillations, before concluding in §6.

2. Models, analysis methods and forcing conditions

We consider a constant-area duct, open at both ends, containing a two-dimensional slot-stabilized laminar premixed flame at a distance x_f from one end. This thermo-acoustic system is modelled identically to that of our previous study (Kashinath *et al.* 2014, §2): (i) the acoustics is treated linearly – because the perturbation Mach number remains small even for large acoustic velocity fluctuations (Dowling 1997) – and its governing equations are discretized with the Galerkin method. (ii) The premixed flame, which is the main source of nonlinearity in this system, is described by a kinematic model based on the level-set approach, known as the *G*-equation in combustion (for details, see Williams 1994):

$$\frac{\partial G}{\partial \tilde{t}} + \tilde{U}\frac{\partial G}{\partial \tilde{x}} + \tilde{V}\frac{\partial G}{\partial \tilde{y}} = s_L \sqrt{\left(\frac{\partial G}{\partial \tilde{x}}\right)^2 + \left(\frac{\partial G}{\partial \tilde{y}}\right)^2}. \tag{2.1}$$

Here tildes denote dimensional values, $G(\tilde{x}, \tilde{y}, \tilde{t})$ is a time-varying function that is negative in the unburnt gas, positive in the burnt gas and zero on the flame surface,
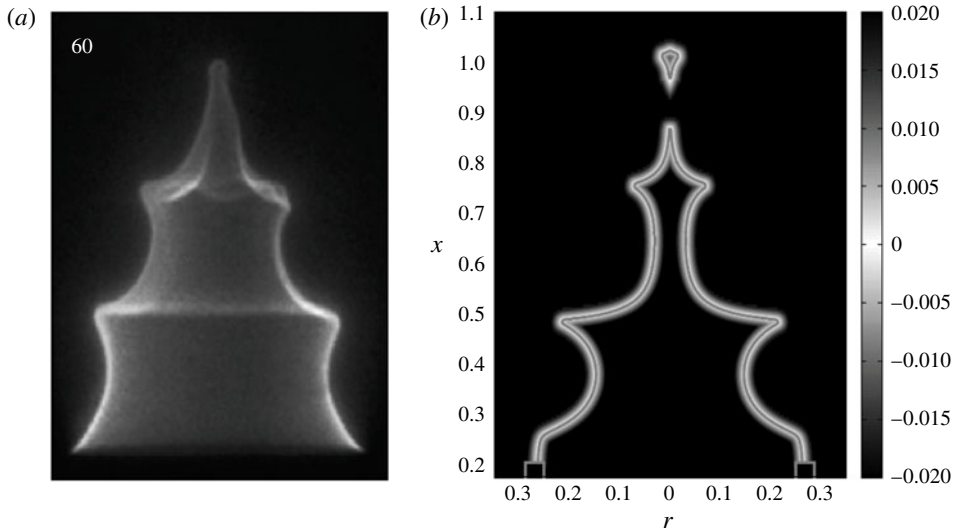
FIGURE 1. Flame wrinkling due to vortex formation and roll-up. (*a*) Experimental image of a forced conical flame. (Reprinted from Karimi *et al.* (2009) with permission from Elsevier.) (*b*) The *G*-field obtained from numerical simulations of a forced conical flame. (Reprinted from Orchini *et al.* (2015) with permission from Cambridge University Press.) In both cases, the forcing is harmonic, with the same frequency and amplitude. The flame contour $G = 0$ is highlighted to show that it can qualitatively reproduce the experimental results.

$\tilde{U}$ and $\tilde{V}$ are the instantaneous velocities along the x and y directions, respectively, and s_L is the flame speed. (iii) Finally, the perturbation velocity field is modelled as a travelling wave that originates at the burner lip and propagates downstream according to the one-dimensional advection equation with a constant phase speed (Kashinath *et al.* 2014, equation (2.10)). This perturbation model has been proved to be able to reproduce the characteristic vortex formation at the burner lip and its roll-up along the flame (Orchini, Illingworth & Juniper 2015). This gives rise to flame wrinkling, which modulates the flame surface area and the resultant heat release rate fluctuations (Preetham, Santosh & Lieuwen 2008). Figure 1 shows a qualitative comparison of the numerically simulated *G*-field against experimental results.

We acoustically force this system by applying a harmonic velocity perturbation at the burner lip. This type of forcing may be achieved in reality using an actuator, such as a loudspeaker. Note that there is no perturbation to the geometry of the system but only to the velocity and pressure fields. The total velocity perturbation at this location is the sum of the self-excited oscillations and the forced perturbations, which may be added together because the acoustics is linear. The flame therefore experiences the combined effect of the self-excited oscillations and the forced perturbations. The net perturbations propagate along the flame surface according to the advection equation (Kashinath *et al.* 2014, equation (2.10)).

The evolution equations of this low-order coupled nonlinear dynamical system (i.e. the acoustic equations, the *G*-equation and the perturbation velocity equations) are solved simultaneously using a weighted essentially non-oscillatory (WENO) fifth-order scheme in space (Jiang & Peng 2000) with a third-order total variation diminishing (TVD) Runge–Kutta scheme (Gottlieb & Shu 1998) in time. The details of these

computations, including the local level-set algorithm used to solve the *G*-equation (Hemchandra 2009), can be found in our previous study (Kashinath *et al.* 2014, §2).

A full description of the synchronization dynamics of this system requires the determination of its Arnold tongues and the bifurcations around them. In this study, we focus on the primary (1 : 1) Arnold tongue (i.e. $f_f \approx f_n$) because it is the widest and hence the easiest to resolve. The forcing frequency, f_f/f_n, is varied from 0.85 to 1.15 in steps of 0.01, with a higher resolution of 0.001 for $0.98 < f_f/f_n < 1.02$. Here f_n is the natural (self-excited) frequency, which is defined as (i) the frequency of the limit cycle of a periodic oscillation, or (ii) one of the two characteristic frequencies of the 2-torus of a quasi-periodic oscillation, or (iii) the dominant frequency in the spectrum of a chaotic oscillation. The forcing amplitude, u'_f, normalized by the mean flow velocity, U_0, given by $\epsilon \equiv u'_f/U_0$, is varied from 0.01 to 0.60 in steps of 0.01. This range is sufficient to achieve lock-in for all the f_f values used in this study.

The response of the system is examined via the pressure fluctuation at a fixed duct location ($x = 0.375$), which is away from the pressure nodes of the dominant acoustic modes. At each forcing condition, we produce a time series lasting 400 steady-state cycles of the fundamental acoustic mode, which is long enough to resolve the low-frequency modulations arising when the system is near its synchronization boundaries. It is worth mentioning that complex behaviour could arise during the transient stages of the simulations, as was observed in our previous study (Kashinath *et al.* 2014). Nevertheless, the focus of the present study is on the steady-state dynamics.

For a periodically forced self-excited system with a single oscillatory mode, two types of synchronization can occur: phase trapping and phase locking (Pikovsky *et al.* 2003). In this study, we use the term 'lock-in' to refer to phase locking, which occurs when a forced self-excited system has a constant phase difference with respect to the forcing at all instants in time. This means that the system always oscillates at f_f. Phase trapping, also known as frequency locking without phase locking, occurs when the phase difference oscillates boundedly around a fixed value as though it is trapped (Aronson, Ermentrout & Kopell 1990). The instantaneous frequency of the system is therefore not always equal to f_f but its time-averaged frequency is. To distinguish between phase locking and phase trapping, we extract the instantaneous phase and amplitude of the pressure signal using the Hilbert transform (Gabor 1946). This technique has the advantage that it can be applied to nonlinear and non-stationary data. Its usefulness in the study of nonlinear dynamics and synchronization is well recognized (Pikovsky *et al.* 2003).

The dynamics of self-excited thermoacoustic systems and the phenomenon of synchronization are governed by nonlinear processes and cannot be described with linear tools. We therefore use methods from dynamical systems theory and nonlinear time-series analysis. These methods are well established and have been documented in textbooks (Strogatz 1994; Thompson & Stewart 2002; Kantz & Schreiber 2003; Small 2005).

3. The unforced self-excited system

The dynamics of the unforced self-excited system were characterized by Kashinath *et al.* (2014). From figure 3 of that paper, we choose four states (corresponding to four different flame positions x_f) at which to study the forced response of the system. These four states are described in table 1. Their time series, power spectra, phase portraits, Poincaré sections, correlation dimensions and instantaneous flame images were shown by Kashinath *et al.* (2014) and are not reproduced here for the sake

State	x_f	Oscillation type	Natural frequency	Preceding bifurcation
A	0.166	Period-1	$f_n = 2.304$	Supercritical Hopf
B	0.480	Period-1	$f_n = 1.125$	Subcritical Hopf
C	0.400	Quasi-periodic	$f_1 = 2.22,\ f_2 = 0.17$	Neimark–Sacker (torus-birth)
D	0.067	Chaotic	$f_n = 1.16$	—

TABLE 1. The natural (unforced) states of the system to which harmonic forcing is applied. These states are reached by varying the flame position x_f within a constant-area duct with open ends, whilst keeping all other parameters constant (Kashinath *et al.* 2014, see figure 3 for details). The natural frequency is non-dimensionalized by the frequency of the fundamental acoustic mode in the absence of heat release and damping.

of conciseness. We choose these particular states because: (i) they are representative of the different types of oscillations present in this thermoacoustic system; (ii) they include limit cycles due to both subcritical and supercritical Hopf bifurcations of the steady base state; and (iii) their amplitudes are small enough that lock-in may be achieved with moderate forcing amplitudes, justifying the attachment boundary condition used for the flame's base (Kashinath *et al.* 2014, §2.3).

4. Forcing of period-1 oscillations: states A and B

In this section, we examine the forced response of the system during period-1 oscillations, which arise from supercritical (state A) or subcritical (state B) Hopf bifurcations of the steady base state. We consider forcing conditions leading up to lock-in for f_f above and below f_n, both close to and far from f_n, i.e. f_f/f_n between 0.95 and 1.05 (close to) and between 0.85 and 1.15 (far from). We also examine the response when the forcing amplitude (ϵ) increases beyond that which is required for lock-in. In all cases, the data shown represent the system's dynamics after reaching steady state. At each forcing condition, we produce a time series lasting 400 steady-state cycles of the fundamental acoustic mode, which is long enough to resolve the low-frequency modulations arising when the system is near its synchronization boundaries. It is worth mentioning that complex behaviour could arise during the transient stages of the simulations, as was observed in our previous study (Kashinath *et al.* 2014, §6). Nevertheless, the focus of the present study is on the steady-state dynamics.

4.1. *Before lock-in: f_f close to f_n*

First we force the system at a frequency close to its natural frequency: $f_f/f_n = 0.98$. The responses for states A and B are qualitatively similar to each other, so for brevity only state A is presented here: a period-1 oscillation arising from a supercritical Hopf bifurcation (Kashinath *et al.* 2014, figure 3 at $x_f = 0.166$). Figure 2 shows the time series and Poincaré maps for this state at different forcing amplitudes (ϵ).

When forced, the system responds at both its natural frequency and the forcing frequency but, as will be shown later, the former (f_n', where the prime indicates the presence of forcing) shifts towards the latter (f_f) and is therefore no longer equal to the natural frequency of the unforced system (f_n). The oscillations in figure 2(*a–f*) are quasi-periodic and arise from a torus-birth bifurcation (i.e. a Neimark–Sacker bifurcation) of the unforced period-1 oscillation. The power spectrum, which is not shown here but is similar to that reported for forced self-excited hydrodynamic systems (Li & Juniper 2013*a,b*), contains peaks at linear combinations of f_n' and f_f,
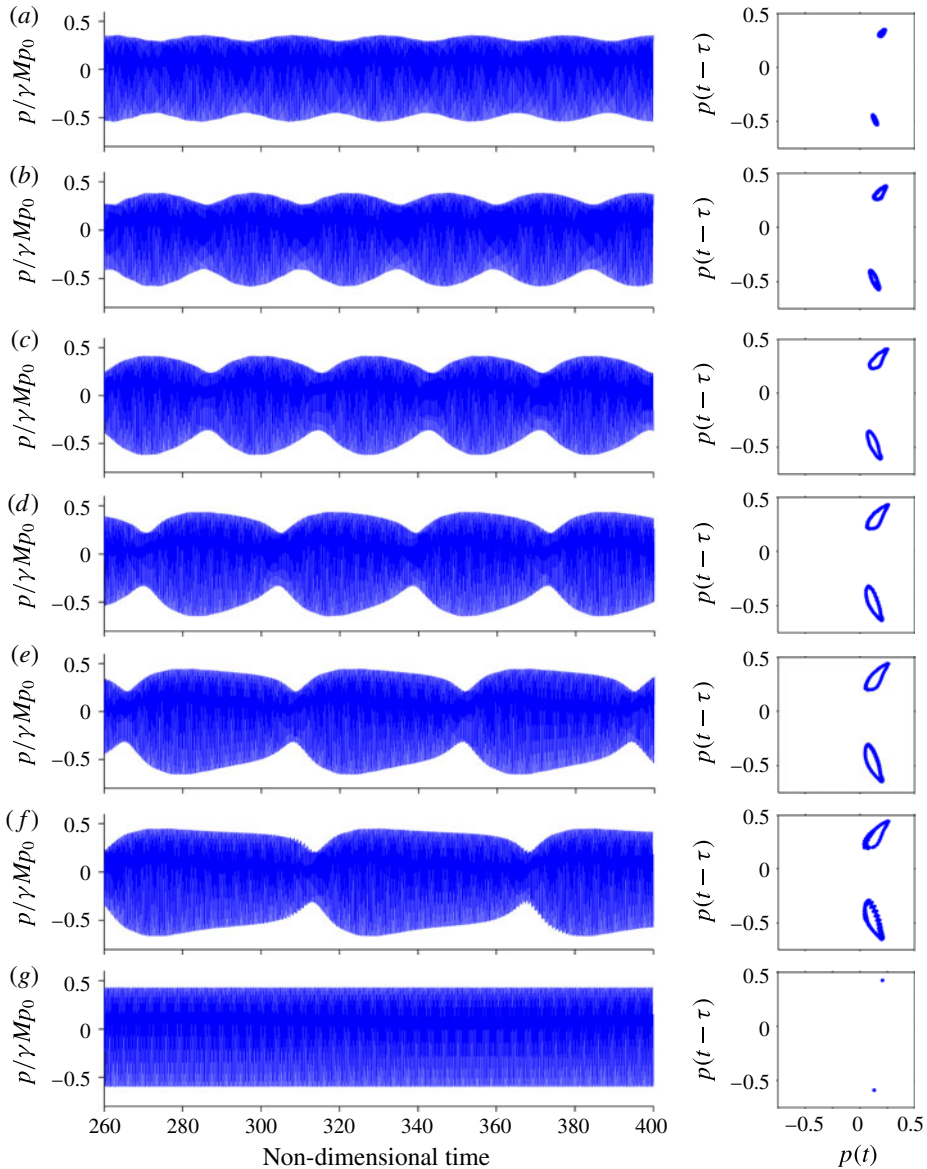
FIGURE 2. (Colour online) Saddle-node bifurcation to lock-in: the forced response of the system during period-1 oscillations (state A) when the forcing frequency is close to the natural frequency, $f_f/f_n = 0.98$, where $f_n = 2.304$. Time series and Poincaré maps are shown for increasing forcing amplitudes: (a) $\epsilon \equiv u'_f/U_0 = 0.03$, (b) 0.06, (c) 0.09, (d) 0.11, (e) 0.12, (f) 0.125 and (g) 0.13.

indicating nonlinear triad interactions between the natural and forced modes. The Poincaré maps show two rings, indicating that the phase trajectory is not closed but spirals around the surface of a stable ergodic 2-torus. The time series shows evidence of beating, a low-frequency modulation of the pressure amplitude at the beating frequency, $\Delta f = f'_n - f_f$.
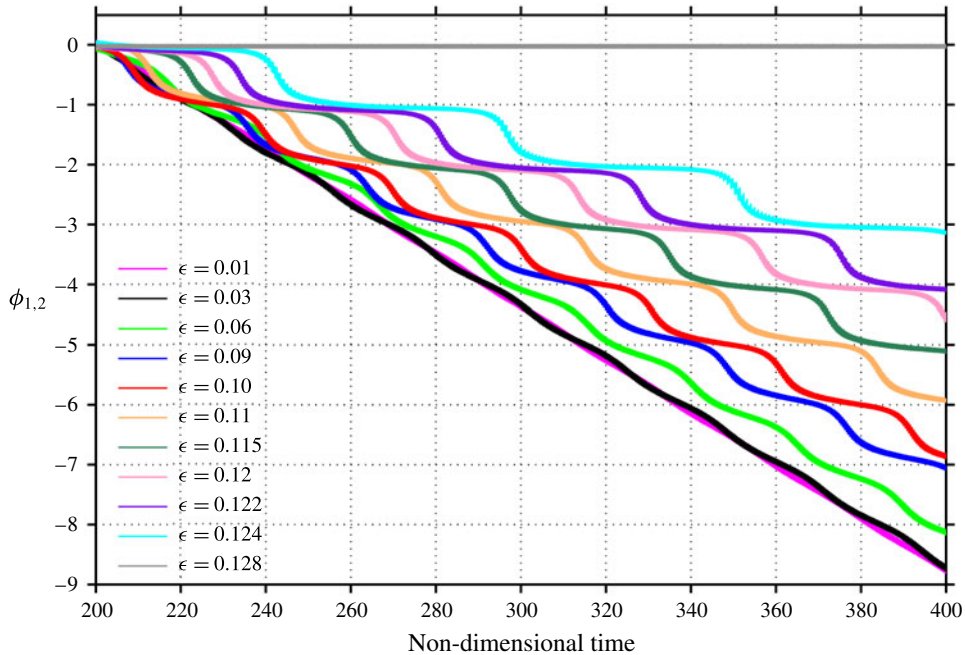
FIGURE 3. (Colour online) Saddle-node bifurcation to lock-in: the phase difference (normalized by 2π) between the system and the forcing at the conditions of figure 2.

When forced above a critical amplitude (figure 2g, $\epsilon = 0.13$), the system locks in to the forcing and oscillates only at f_f. The Poincaré map shows two discrete points, indicating a closed period-1 orbit in phase space. This transition from a quasi-periodic oscillation to a period-1 oscillation is abrupt, which, as will be confirmed later, reveals a saddle-node bifurcation to lock-in. The attractor at lock-in is a stable periodic orbit on the surface of the 2-torus that existed before the saddle-node bifurcation (Balanov *et al.* 2009).

Figure 3 shows the phase difference $\phi_{1,2}$ (normalized by 2π) between the system and the forcing at the conditions of figure 2. The response pressure is measured at the same position in the duct as the forcing (i.e. the burner lip). Furthermore, we assume acoustic compactness of the flame. Different x positions in the duct will have different phase, but focusing on one location is sufficient to understand the complete dynamics because other locations will behave similarly with a constant (time-invariant) phase difference. To explore the different states of synchronization, it is necessary to consider only the temporal evolution of $\phi_{1,2}$ and not its absolute value (Pikovsky *et al.* 2003). The average slope of each curve is the beating frequency, $\Delta f = f'_n - f_f$. In all cases except at $\epsilon = 0.128$ (strong forcing), the oscillations are quasi-periodic, as indicated by the non-zero slope of $\phi_{1,2}$, showing that $f'_n \neq f_f$. As ϵ increases, two trends emerge. First, the linear decrease in $\phi_{1,2}$ becomes increasingly wavy, with alternating periods of synchronicity (flat slope) and asynchronicity (steep slope), the latter of which are called phase slips (Pikovsky *et al.* 2003). Second, the magnitude of the average slope of each curve decreases, indicating that $f'_n \rightarrow f_f$. This behaviour, called frequency pulling, is characteristic of lock-in via a saddle-node bifurcation and can be modelled with universal low-dimensional oscillators (Balanov *et al.* 2009).

With strong forcing ($\epsilon \geqslant 0.12$), there are times when $\phi_{1,2}$ is nearly constant, indicating synchronicity, with phase slips occurring relatively abruptly. The phase slips are equal to -2π because here $f_f/f_n < 1$, which means that the system overtakes the forcing by one full cycle during a phase slip. As ϵ increases further, both the abruptness of the phase slips and the time interval between them increase, ultimately leading to infinitely long intervals of constant $\phi_{1,2}$ and thus lock-in.

The characteristics observed in figures 2 and 3, which correspond to $f_f < f_n$, are also observed when $f_f > f_n$ as long as f_f is close to f_n. Crucially, the sequence of bifurcations remains unchanged: it begins with a torus-birth bifurcation to quasi-periodicity from a period-1 oscillation, followed by a saddle-node bifurcation to lock-in at a critical forcing amplitude. However, when $f_f > f_n$, the phase slips occur in the opposite direction ($+2\pi$) because the system loses one full cycle with respect to the forcing when it phase slips.

4.2. *Before lock-in: f_f far from f_n*

Next we force the system at a frequency far from its natural frequency: $f_f/f_n = 0.89$. For completeness, here we present state B, which responds qualitatively similarly to state A and is likewise a period-1 oscillation. However, state B arises from a subcritical, rather than a supercritical, Hopf bifurcation of the steady base state (Kashinath *et al.* 2014, figure 3). Figure 4 shows the time series, power spectra and phase portraits for this state at increasing ϵ, starting with the unforced case (figure 4*a*).

Compared to figure 2 (f_f close to f_n), figure 4 (f_f far from f_n) shows many similarities but also some key differences. In both cases, at intermediate forcing amplitudes, the system responds at both f_n' and f_f, becoming quasi-periodic via a torus-birth bifurcation of the unforced period-1 oscillation. Furthermore, the time series show low-frequency beating and the phase portraits show a stable ergodic 2-torus.

For f_f far from f_n (figure 4), f_n' remains unchanged from its unforced value (f_n) as ϵ increases; but for f_f close to f_n (§ 4.1), f_n' shifts towards f_f, leading to frequency pulling. Moreover, for f_f far from f_n, the power spectra show a steady decrease in the amplitude of the natural mode (at f_n') and a corresponding increase in the amplitude of the forced mode (at f_f). At lock-in (figure 4*h*), the system oscillates only at f_f, with the natural mode becoming suppressed and the phase trajectory in a closed period-1 orbit, similar to the case for f_f close to f_n (figure 2*g*). However, unlike for f_f close to f_n, here the transition from quasi-periodicity to lock-in is gradual rather than abrupt, revealing an inverse Neimark–Sacker bifurcation (i.e. a torus-death bifurcation) rather than a saddle-node bifurcation. This is consistent with predictions from generic models of self-excited oscillators, such as the forced van der Pol oscillator (Balanov *et al.* 2009). Finally, the response amplitude at lock-in is significantly lower than that of the unforced case; at this particular value of f_f/f_n, it is approximately 70 % lower (compare figure 4*a* with figure 4*h*). As will be discussed in § 4.4, this decrease tends to occur when f_f is far from f_n. When f_f is close to f_n, however, the response amplitude at lock-in tends to be higher than that of the unforced case. Nevertheless, the decrease shows that weakening of self-excited thermoacoustic oscillations is possible via open-loop acoustic forcing at far-off-resonance frequencies, confirming the results of Bellows *et al.* (2008).

Figure 5 shows the phase difference $\phi_{1,2}$ (normalized by 2π) at the conditions of figure 4. For weak forcing ($0 < \epsilon \leqslant 0.14$), $\phi_{1,2}$ decreases linearly with an average slope
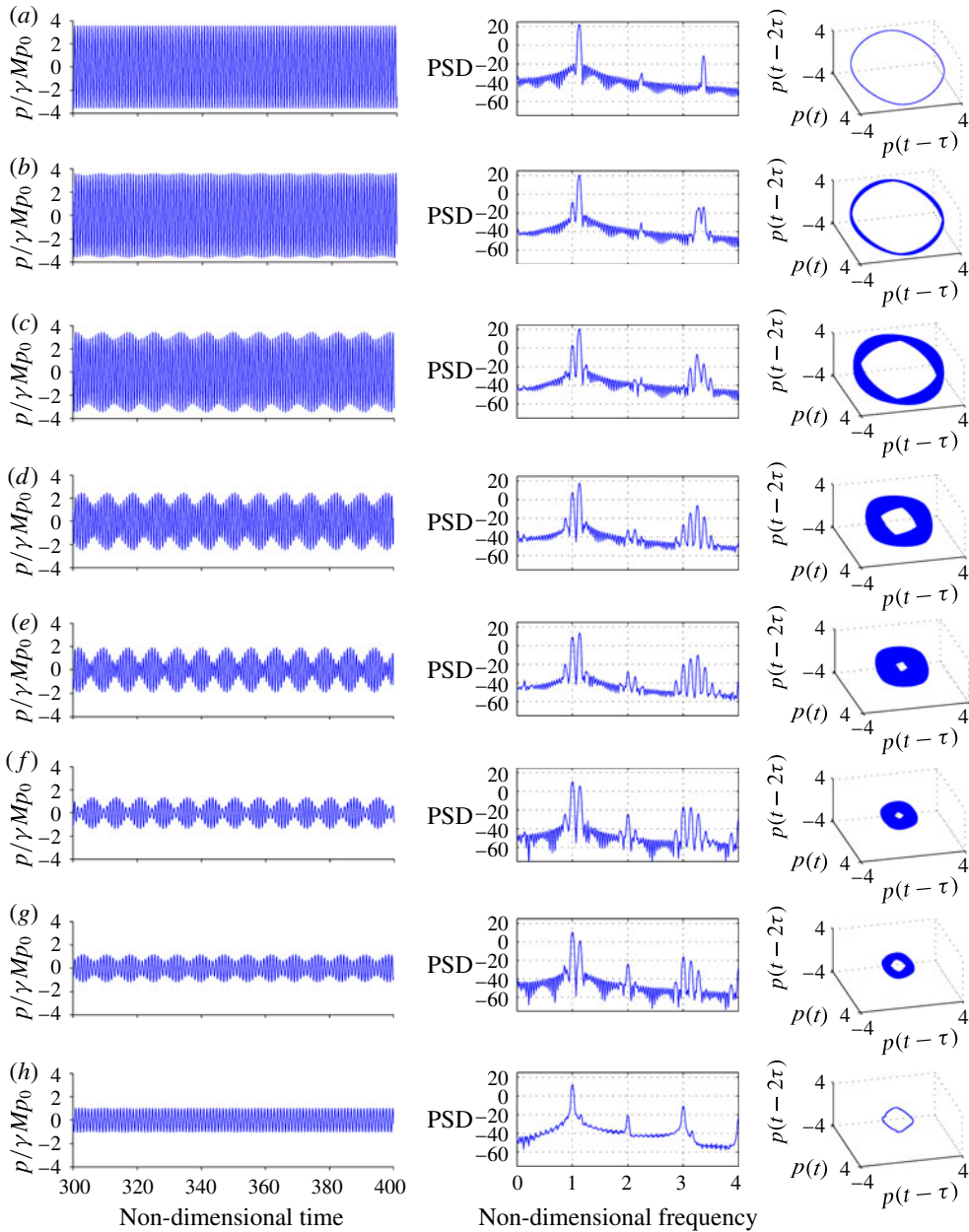
FIGURE 4. (Colour online) Torus-death bifurcation to lock-in: the forced response of the system during period-1 oscillations (state B) when the forcing frequency is far from the natural frequency, $f_f/f_n = 0.89$, where $f_n = 1.125$. Time series, power spectra and phase portraits are shown for increasing forcing amplitudes: (a) $\epsilon \equiv u'_f/U_0 = 0.00$ or unforced, (b) 0.02, (c) 0.08, (d) 0.14, (e) 0.16, (f) 0.18, (g) 0.20 and (h) 0.23.

equal to the beating frequency, $\Delta f = f_f - f'_n$. For moderate forcing ($0.14 < \epsilon \leqslant 0.18$), the magnitude of the average slope increases via large phase slips (many of them $> 2\pi$), indicating frequency pushing: f'_n shifts away from f_f as ϵ increases, which
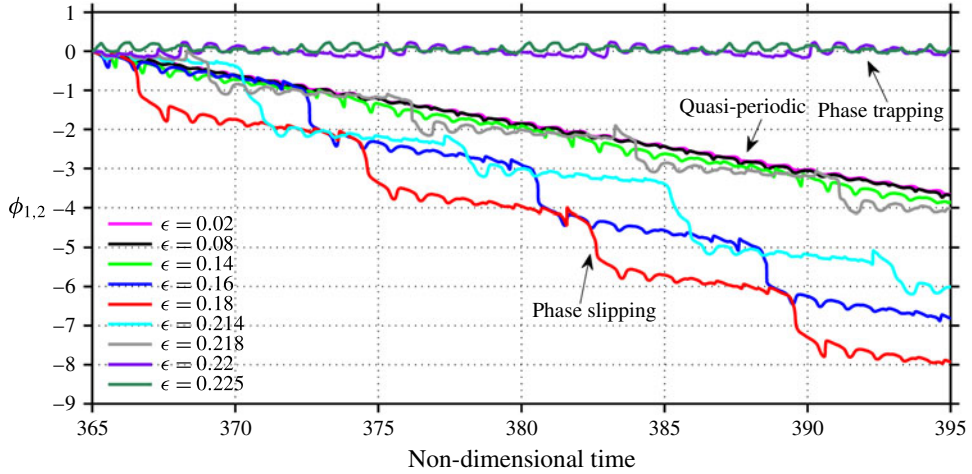
FIGURE 5. (Colour online) Torus-death bifurcation to lock-in: the phase difference (normalized by 2π) between the system and the forcing at the conditions of figure 4.

will be discussed below. For stronger forcing, the magnitude of the average slope decreases slightly ($0.18 < \epsilon \leqslant 0.218$), indicating frequency pulling, before abruptly snapping to zero at $\epsilon = 0.218 \rightarrow 0.22$. After this, the phase slips continue to occur, keeping $\phi_{1,2}$ bounded within a $\pm\pi$ band around $\phi_{1,2} = 0$. The result is a partially synchronous state known as phase trapping (Aronson *et al.* 1990), which was only recently discovered in hydrodynamics (Li & Juniper 2013*c*) and thermoacoustics (Balusamy *et al.* 2015). During phase trapping, the oscillations are still quasi-periodic and frequency-locked but are not phase-locked. They become phase-locked only at lock-in, when the amplitude at f'_n is completely quenched ($\epsilon = 0.23$). In figure 4, this last sequence of events (frequency pulling $\rightarrow$ phase trapping $\rightarrow$ lock-in) coincides with the forced mode overtaking the natural mode in amplitude (figure 4*e–h*) and was recently reported for a forced hydrodynamically self-excited low-density jet (Li & Juniper 2013*c*). It is worth mentioning that, although the results shown in figures 4 and 5 are for $f_f < f_n$, the same qualitative behaviour is seen for $f_f > f_n$ as long as f_f is far from f_n.

The phenomenon of frequency pushing has been observed by Bellows *et al.* (2008) and Balusamy *et al.* (2015) in experiments on lean-premixed turbulent combustors at similar forcing conditions, i.e. for f_f far from f_n. Those researchers mentioned that this shift in the natural frequency could not be explained simply. Frequency pushing is well known, however, in magnetrons (Chen 1990) and has been modelled successfully by adding a Duffing (cubic restoring force) term to the van der Pol equation (Walsh *et al.* 1989). In magnetrons, frequency pushing arises from highly nonlinear electron–wave interactions that change the mean field (Chen 1990). Given the similarities between this thermoacoustic system and universal model oscillators, we speculate that frequency pushing in thermoacoustics could also be modelled by adding a Duffing term.

4.3. *Before lock-in: beating frequency and summary*

For a closer examination of the beating frequency, figure 6 shows the dependence of $\Delta f = f_f - f'_n$ on f_f, both normalized by f_n at two different values of ϵ. The data
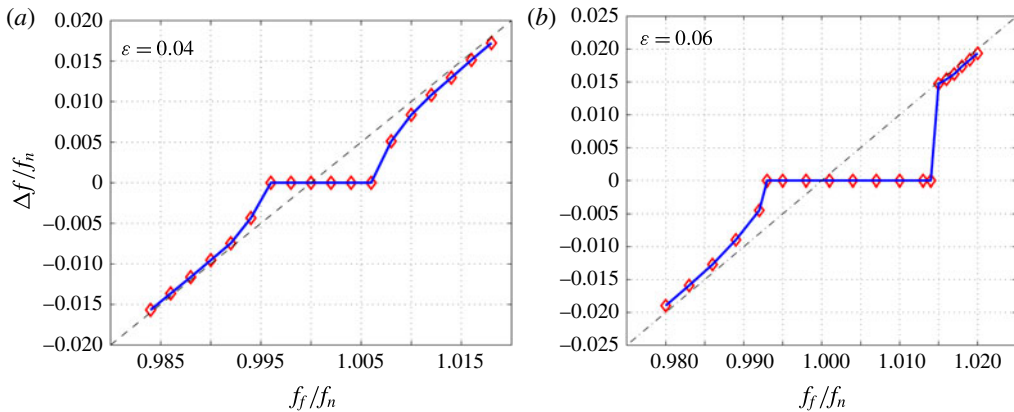
FIGURE 6. (Colour online) Dependence of the beating frequency, $\Delta f = f_f - f'_n$, on the forcing frequency, f_f, both normalized by the unforced natural frequency, f_n, at two forcing amplitudes: (a) $\epsilon = 0.04$, where lock-in occurs via a saddle-node bifurcation for both $f_f < f_n$ and $f_f > f_n$, and (b) $\epsilon = 0.06$, where lock-in occurs via a saddle-node bifurcation for $f_f < f_n$ but via a torus-death bifurcation for $f_f > f_n$.

shown are for state B but are also representative of state A. In figure 6(a), where the forcing is weak ($\epsilon = 0.04$), $\Delta f/f_n$ around $f_f/f_n = 1$ is zero, indicating lock-in. For higher or lower values of f_f/f_n, the magnitude of $\Delta f/f_n$ increases (i) nonlinearly close to the lock-in boundary, indicating frequency pulling, but (ii) linearly away from it, indicating no frequency pulling. This behaviour of $\Delta f/f_n$ has been derived analytically for low-order model oscillators and is well known in the literature of nonlinear dynamics and synchronization (Pikovsky *et al.* 2003): $\Delta f/f_n$ has a square-root dependence on frequency detuning ($f_f - f_n$) close to the saddle-node bifurcation, where f_f is relatively close to f_n. In figure 6(a), an approximately square-root dependence is seen on both sides of $f_f/f_n = 1$.

Figure 6(b) is with stronger forcing ($\epsilon = 0.06$). As in figure 6(a), $\Delta f/f_n$ is zero near $f_f/f_n = 1$ (indicating lock-in) and has a similar square-root-like dependence when $f_f/f_n < 1$ (indicating frequency pulling). However, when $f_f/f_n > 1$, $\Delta f/f_n$ increases (i) abruptly at the lock-in boundary and (ii) linearly away from it, indicating an absence of frequency pulling. This suggests that, at this particular forcing amplitude ($\epsilon = 0.06$), lock-in occurs via a torus-death bifurcation when $f_f/f_n > 1$ but via a saddle-node bifurcation when $f_f/f_n < 1$. This will be confirmed in §4.4.

In summary, we have shown that, even when oscillating periodically, this self-excited thermoacoustic system responds to harmonic forcing in many different ways, depending on the proximity of the forcing frequency (f_f) to the natural frequency (f_n) and whether f_f is above or below f_n. When the forcing amplitude (ϵ) increases from zero, the system first undergoes a torus-birth bifurcation to quasi-periodicity from a period-1 oscillation. When ϵ exceeds a critical value, the system locks in to the forcing. If f_f is close to f_n, lock-in occurs via a saddle-node bifurcation with frequency pulling. If f_f is far from f_n, lock-in occurs via a torus-death bifurcation, with frequency pushing if f_f and f_n are sufficiently far apart. The lock-in process has two subtle features: (i) it is asymmetric about $f_f/f_n = 1$ and (ii) the response amplitude at lock-in may be larger or smaller than that of the unforced system. These and other lock-in features will be discussed next.
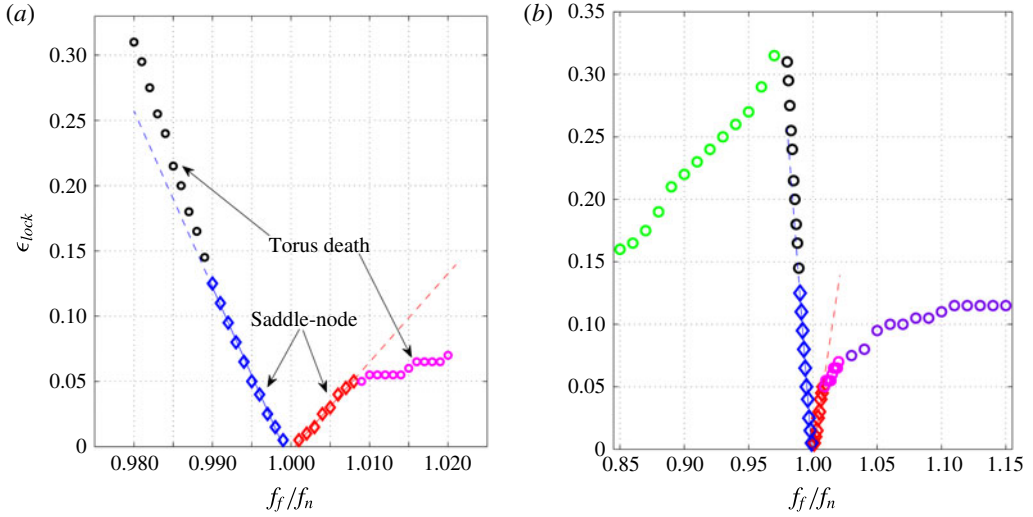
FIGURE 7. (Colour online) The $1:1$ Arnold tongue for period-1 oscillations (state B) when forced across (*a*) a small range of frequency detuning ($0.98 < f_f/f_n < 1.02$) and (*b*) a large range of frequency detuning ($0.85 < f_f/f_n < 1.15$). The diamond markers denote saddle-node bifurcations, and the circular markers denote torus-death bifurcations. The dashed lines are linear fits to the saddle-node data on either side of $f_f/f_n = 1$.

4.4. *At lock-in: the 1:1 Arnold tongue, response amplitudes and jump phenomena*

In this section, we continue to examine the system during period-1 oscillations (state B), but we focus on the forced response at lock-in. Figure 7 shows the $1:1$ Arnold tongue: the minimum forcing amplitude required for lock-in, ϵ_{lock}, as a function of the frequency detuning around $f_f/f_n = 1$. The diamond markers denote saddle-node bifurcations, and the circular markers denote torus-death bifurcations. The dashed lines are linear fits to the saddle-node data on either side of $f_f/f_n = 1$.

In figure 7(*a*), ϵ_{lock} increases linearly with $|f_f - f_n|$ when f_f is close to f_n, producing a characteristic V-shaped lock-in curve for saddle-node bifurcations. Similar V-shaped curves have been reported for other self-excited, but physically disparate, systems such as turbulent lean-premixed combustors (Bellows *et al.* 2008), momentum-dominated low-density jets (Li & Juniper 2013*a*), laminar jet diffusion flames (Li & Juniper 2013*b*), low-density and equidensity cross-flowing jets (Davitian *et al.* 2010; Getsinger, Hendrickson & Karagozian 2012), capillary jets (Olinger 1992) and cylinder wakes (Provansal, Mathis & Boyer 1987). The slope of the V is asymmetric about $f_f/f_n = 1$: lock-in occurs more readily for $f_f/f_n > 1$ than for $f_f/f_n < 1$. A similar asymmetry has been observed in laminar jet diffusion flames (Li & Juniper 2013*b*) and equidensity cross-flowing jets (Davitian *et al.* 2010), but an opposite asymmetry has been observed in cylinder wakes (Blevins 1985), low-density cross-flowing jets (Getsinger *et al.* 2012) and momentum-dominated low-density jets (Li & Juniper 2013*a*). The exact cause of the asymmetry is unknown.

The boundary between saddle-node and torus-death bifurcations lies closer to $f_f/f_n = 1$ when $f_f/f_n > 1$. Beyond this boundary, the loci of the torus-death bifurcations deviate from the linear fits to the saddle-node data, which is a trend that has been proved analytically for the forced van der Pol oscillator (Holmes & Rand 1978). Furthermore, the loci of the torus-death bifurcations are different on either side of $f_f/f_n = 1$ (i.e. the
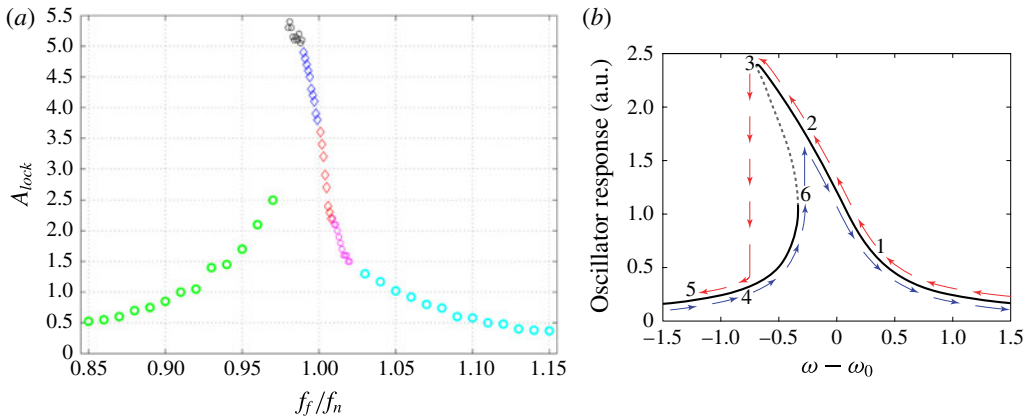
FIGURE 8. (Colour online) (*a*) The system response at lock-in, i.e. at the critical forcing amplitude, ϵ_{lock}. The response is defined as the non-dimensional amplitude of the pressure oscillations, $A_{lock} = p'/\gamma M p_0$. As in figure 7(*b*), the diamond markers denote saddle-node bifurcations, and the circular markers denote torus-death bifurcations, with the different colours indicating different regimes. (*b*) The frequency-response curve for a forced Duffing oscillator with a soft cubic spring. The dashed branch (between points 3 and 6) is unstable and cannot be reached in experiments or simulations, leaving a discontinuous jump that resembles that seen in panel (*a*).

left and right branches of the 1 : 1 Arnold tongue). Figure 7(*b*) shows the same Arnold tongue as figure 7(*a*) but over a larger range of f_f/f_n. The data for $f_f/f_n > 1$ (right branch) saturate at $\epsilon_{lock} \approx 0.12$, but the data for $f_f/f_n < 1$ (left branch) peak at $\epsilon_{lock} \approx 0.32$ (where $f_f/f_n \approx 0.97$) before decreasing with decreasing f_f/f_n. This behaviour of the left branch is identical to that seen in experiments on hydrodynamically self-excited jet diffusion flames (Li & Juniper 2013*b*). It is attributed to subharmonic lock-in arising from the overlap of the adjacent 3 : 4 Arnold tongue.

Figure 8(*a*) shows the response amplitude of the system at lock-in (i.e. at ϵ_{lock}) as a function of f_f/f_n. Here the response amplitude is defined as the non-dimensional amplitude of the pressure oscillations, $A_{lock} = p'/\gamma M p_0$. The peak in A_{lock} at a frequency below $f_f/f_n = 1$ and the sharp decrease on either side of it give rise to a characteristic 'shark-fin' curve that has been observed in other nonlinear systems, such as hydrodynamically self-excited jet diffusion flames (Li 2012) and thermoacoustically self-excited turbulent premixed flames (Bellows *et al.* 2008). Crucially, this behaviour is also observed in the forced response of low-dimensional model oscillators, such as the Duffing oscillator with a soft cubic spring (Thompson & Stewart 2002). This similarity in the forced response of physically disparate systems is further evidence that, with more analysis, some aspects of thermoacoustically self-excited systems can be represented by simple model oscillators.

A discontinuous jump in A_{lock} occurs at a critical value of f_f/f_n (0.97), suggesting a region of bistability and the possibility of hysteresis. This jump phenomenon is a classical feature of a cusp catastrophe (Thompson & Stewart 2002). It arises when variations in one or two of the control parameters (here f_f and ϵ) cause the system to cross the fold curve on the catastrophe surface, jumping from a point on the upper (lower) stable manifold to a point on the lower (upper) stable manifold (Nayfeh & Mook 1995). To produce figure 8(*a*), we started the simulations at $f_f/f_n = 1$ and worked outwards, increasing f_f to get to $f_f/f_n > 1$ and decreasing f_f to get to $f_f/f_n < 1$.

Hence, the bifurcation at $f_f/f_n = 0.97$ is reached by decreasing f_f. This corresponds to path $1 \rightarrow 2 \rightarrow 3 \rightarrow 4 \rightarrow 5$ in figure 8(*b*), which is a sketch of the frequency-response curve for a forced Duffing oscillator with a soft cubic spring (Nayfeh & Mook 1995). The reverse path $5 \rightarrow 4 \rightarrow 6 \rightarrow 2 \rightarrow 1$ is not explored in this study, but is expected to extend the lower branch of figure 8(*a*) (green circles) further to the right.

Like the V-shaped lock-in curve and the 'shark-fin' frequency-response curve, the jump phenomenon has been observed in various nonlinear systems, such as electronic circuits (Giannakopoulos & Deliyannis 2001), hypoid gears (Wang & Lim 2011), ecosystems (Scheffer *et al.* 2001), shape-memory alloys (Xia & Sun 2015) and turbulent premixed combustors (Bellows *et al.* 2008). Crucially, it can be modelled accurately with a forced Duffing oscillator, a second-order nonlinear damped oscillator with cubic elasticity subjected to periodic forcing (Nayfeh & Balachandran 2004):

$$\ddot{x} + 2\zeta\omega_0\dot{x} + \omega_0^2 x + \beta x^3 = \epsilon\cos(\omega_f t). \qquad (4.1)$$

Here x is the position at time t, ζ is the damping constant, ω_0 is the undamped natural frequency and β controls the degree of nonlinearity in the restoring force. On the right-hand side, ϵ is the forcing amplitude and ω_f is the angular frequency of the forcing. Figure 8(*b*) shows the typical frequency-response curve for a forced Duffing oscillator with a soft cubic spring ($\beta < 0$). The dashed branch (between points 3 and 6) is unstable and cannot be reached in experiments or simulations, leaving a discontinuous jump that resembles that seen in figure 8(*a*). The forced Duffing oscillator is also able to reproduce the peak in the response amplitude at $f_f/f_n < 1$, as well as predicting hysteresis. Moreover, when f_f is far from f_n, both the Duffing oscillator and the thermoacoustic system oscillate at amplitudes that are far below those of their unforced states. This implies that it may be possible (i) to use open-loop harmonic forcing to weaken self-excited thermoacoustic oscillations and (ii) to understand and predict how this occurs through analysis of low-order model oscillators. Quantitatively relating the coefficients of such model oscillators to the system characteristics is possible but beyond the scope of this study.

In summary, lock-in occurs most readily when f_f is close to f_n, but the details depend on whether $f_f > f_n$ or $f_f < f_n$. When $f_f < f_n$, stronger forcing is required for lock-in than when $f_f > f_n$. However, when f_f is gradually decreased from f_n, the response amplitude at lock-in first increases, reaches a maximum and then drops abruptly in turn. This jump phenomenon is a well-known hysteretic feature of nonlinear oscillators undergoing a cusp catastrophe. When f_f is far from f_n, the response amplitude at lock-in drops to as low as 10 % of that of the unforced system. This shows that lock-in can be an effective means of weakening self-excited thermoacoustic oscillations, provided that f_f is chosen carefully with respect to f_n. Finally, the similarities in the forced response of this thermoacoustic system and that of universal model oscillators suggest that the behaviour seen here is not limited to this particular system, but is representative of an entire class of self-excited oscillators with a single dominant oscillatory mode.

4.5. *An alternative route to lock-in: intermittency*

In §§ 4.1 and 4.2, we showed that lock-in can occur via a torus-birth bifurcation followed by either (i) a saddle-node bifurcation with frequency pulling or (ii) a torus-death bifurcation without frequency pulling. Although this is true for many types of periodic oscillations, the transition to lock-in may sometimes involve other bifurcations, including transition to chaos. This may arise from large forcing
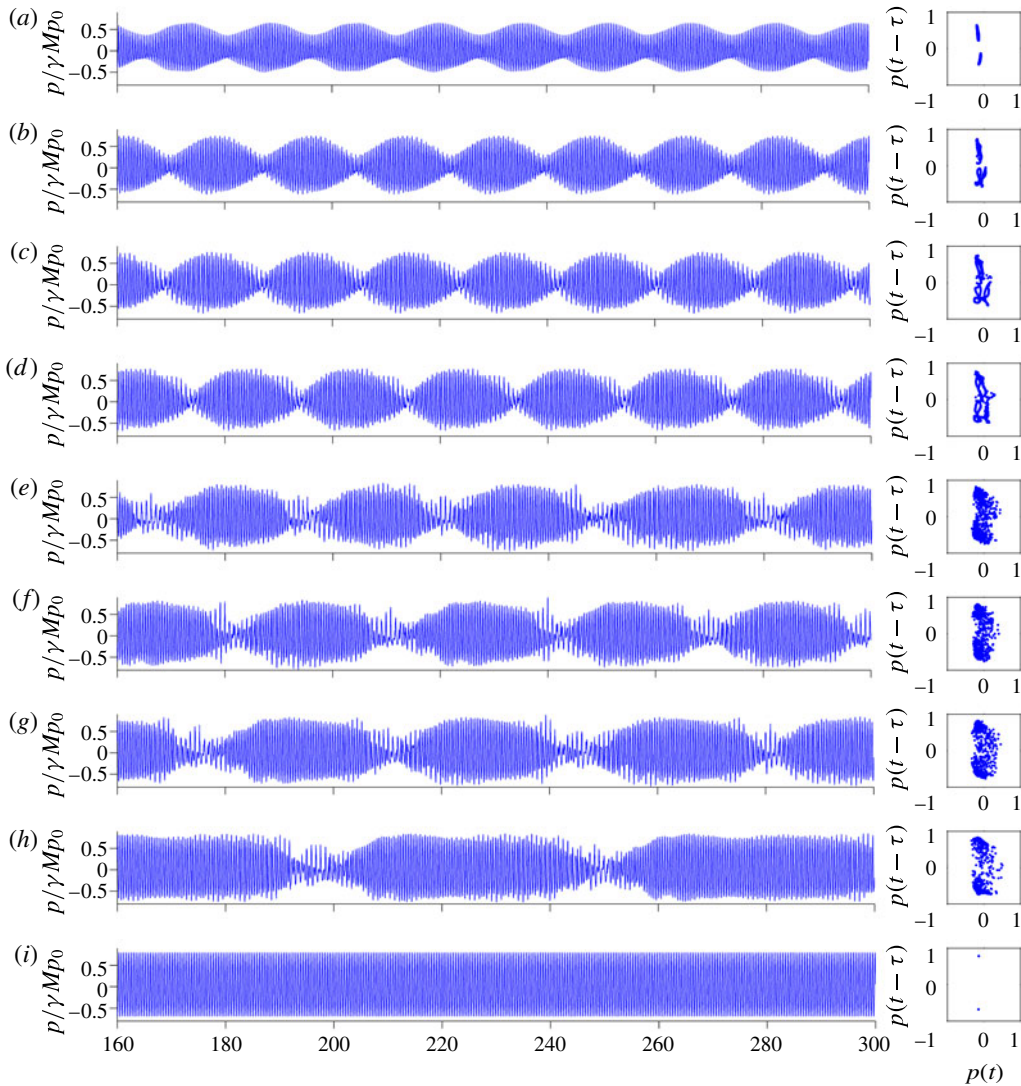
FIGURE 9. (Colour online) Intermittency route to lock-in: the forced response of the system during period-1 oscillations (state A) when $f_f/f_n = 0.97$, where $f_n = 2.304$. Time series and Poincaré maps are shown for increasing forcing amplitudes: (a) $\epsilon \equiv u'_f/U_0 = 0.06$, (b) 0.12, (c) 0.16, (d) 0.18, (e) 0.20, (f) 0.21, (g) 0.22, (h) 0.23 and (i) 0.24.

amplitudes, forcing frequencies far away from the natural frequency or self-excited oscillations that are extremely resistant to external forcing (Pikovsky *et al.* 2003).

Figure 9 shows the transition to lock-in when the system, undergoing period-1 oscillations (state A), is forced at $f_f/f_n = 0.97$. As ϵ increases from zero, the first transition is a torus-birth bifurcation to quasi-periodicity, as seen previously in §§ 4.1 and 4.2. However, this is followed by intermittent instability in the torus attractor: the phase trajectories in a neighbourhood around the surface of the 2-torus start to diverge. In the time series, this appears as mildly chaotic oscillations separated by 'quiet' quasi-periodic intervals, but complete breakdown of the 2-torus to fully chaotic
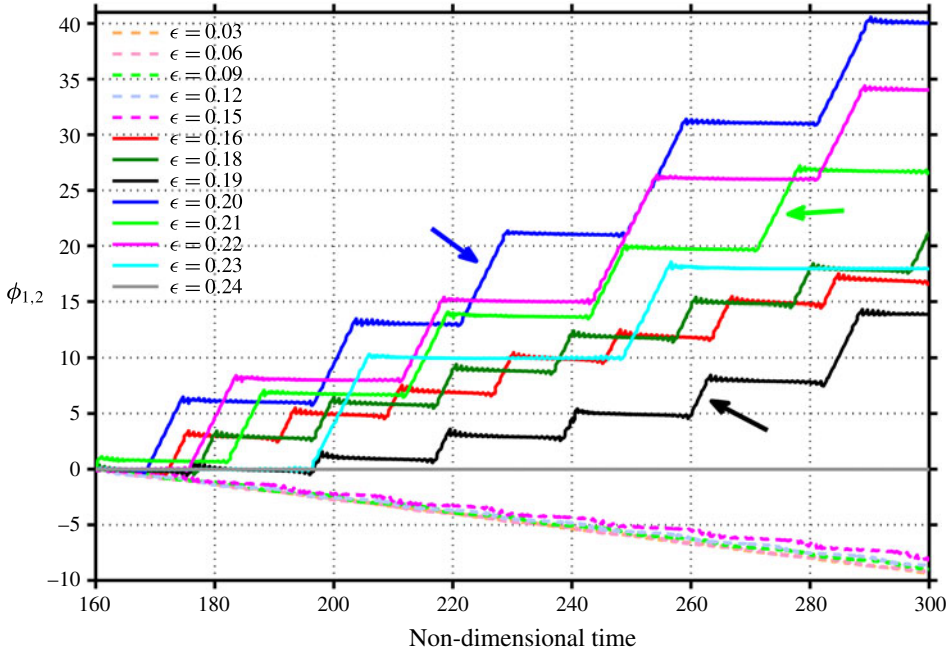
FIGURE 10. (Colour online) Intermittency route to lock-in: the phase difference (normalized by 2π) between the system and the forcing at the conditions of figure 9. The arrows show that phase slips can be greater than 2π.

oscillations does not occur. (It is worth noting that, at a different operating point, complete breakdown to chaos does occur, resembling the Ruelle–Takens–Newhouse route to chaos presented by Kashinath *et al.* (2014).) When ϵ increases further, the mildly chaotic oscillations eventually lock in to the forcing, resulting in period-1 oscillations again but this time at f_f (figure 9*i*).

Figure 10 shows $\phi_{1,2}$ at the conditions of figure 9. As ϵ increases from zero, the magnitude of the slope of $\phi_{1,2}$ decreases, indicating frequency pulling, similar to that seen in figure 3. For $\epsilon > 0.15$ (solid lines), phase slips occur between periods of quasi-periodicity. The arrows show that the phase slips can be greater than 2π and cause the slope of $\phi_{1,2}$ to become positive, producing an overshoot in the frequency pulling that causes the system to oscillate at a frequency slightly higher than that of the forcing, even though $f_f/f_n = 0.97$. Inspection of figures 9 and 10 shows that the phase slips coincide with (i) intervals of intermittent 'spikes' in the time series and (ii) intermittent instability of the phase trajectories around the 2-torus. With stronger forcing ($0.21 \leqslant \epsilon \leqslant 0.23$), the phase slips become more infrequent and, at $\epsilon = 0.24$, the slope of $\phi_{1,2}$ is zero, indicating lock-in.

Intermittency is well-known in synchronization and has been studied extensively in many systems, from simple one-dimensional maps, such as the circle map, to more complex systems of coupled chaotic oscillators (Belair & Glass 1983; Glass *et al.* 1984). The reasons behind the various transitions and their bifurcations have been studied for low-dimensional dynamical systems using periodic orbit theory (Venkatesan & Lakshmanan 1997). A detailed investigation of these transitions and bifurcations in our thermoacoustic system is beyond the scope of this study.
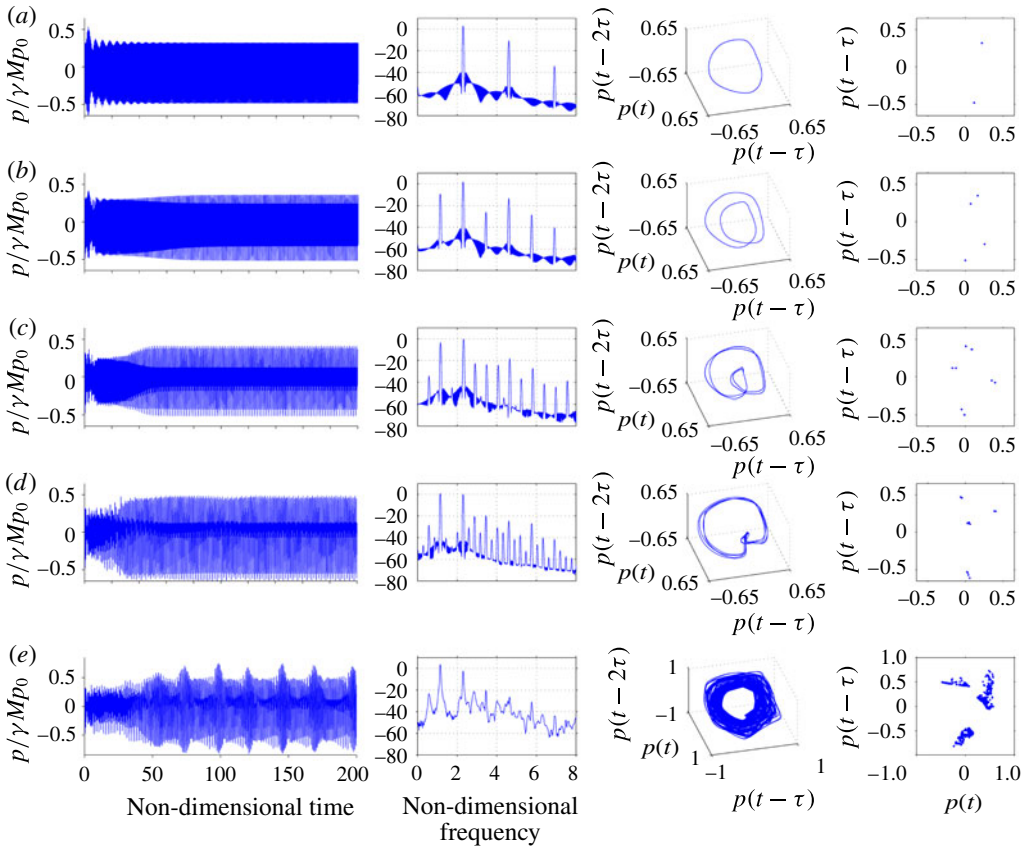
FIGURE 11. (Colour online) Transition to chaos from lock-in via period-doubling bifurcations (route I): the forced response of the system during period-1 oscillations (state B) when $f_f/f_n = 1$, where $f_n = 1.125$. Time series, power spectra, phase portraits and Poincaré maps are shown for increasing forcing amplitudes: (a) $\epsilon \equiv u'_f/U_0 = 0.16$, (b) 0.24, (c) 0.30, (d) 0.34 and (e) 0.36.

4.6. *Beyond lock-in: the stability of synchronized oscillations*

As ϵ increases above ϵ_{lock}, the amplitude of the phase-locked oscillations at f_f also increases. However, for large values of ϵ, the periodic orbit at f_f can become unstable and transition to chaos. Pikovsky *et al.* (2003) explain that there are three main routes to chaos when ϵ increases within an Arnold tongue. Route I, which is typically found near the centre of the Arnold tongue where the stable and unstable periodic orbits are far apart, involves a series of period-doubling bifurcations of the stable periodic orbit. And routes II and III, which are typically found near the outer edges of the Arnold tongue where the frequency detuning is large, involve intermittency, which manifests as long 'laminar' synchronized periods separated by phase slips at chaotic intervals (route II usually occurs at smaller values of ϵ (Pikovsky *et al.* 2003)). All three routes to chaos have been analysed by Afraimovich & Shilnikov (1983) and Aronson *et al.* (1990).

Figure 11 shows an example of route I: transition to chaos via period-doubling bifurcations of the locked-in periodic orbit at f_f. In our previous study, we observed
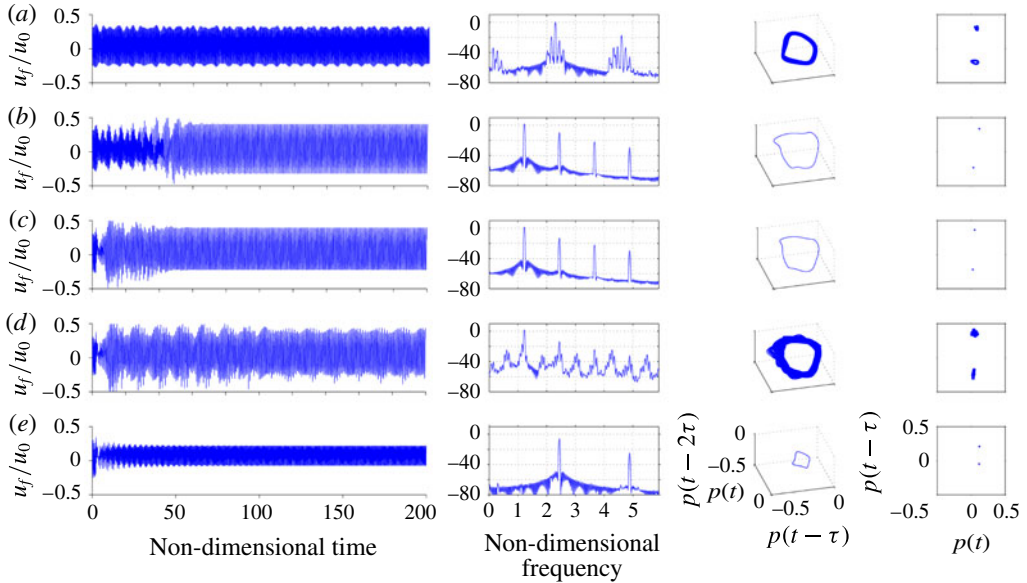
FIGURE 12. (Colour online) Switching between different stable attractors after lock-in: the forced response of the system during period-1 oscillations (state A) when $f_f/f_n = 1.06$, where $f_n = 2.304$. Time series, power spectra, phase portraits and Poincaré maps are shown for increasing forcing amplitudes: (*a*) $\epsilon \equiv u'_f/U_0 = 0.03$, (*b*) 0.16, (*c*) 0.18, (*d*) 0.21 and (*e*) 0.24.

this route to chaos when the flame position was varied (Kashinath *et al.* 2014, figure 14). In figure 11, the same route to chaos is observed when ϵ is increased. The period-1 oscillations (arising from lock-in) undergo a period-doubling bifurcation to period-2 oscillations, followed by another period-doubling bifurcation to period-4 oscillations and so on. The power spectra show the emergence of a new subharmonic at each period-doubling bifurcation: $f_f/2$ in figure 11(*b*), $f_f/4$ in (*c*), $f_f/8$ in (*d*), ultimately leading to chaos in (*e*).

Apart from chaos, there are other features of synchronization at large ϵ that are not observed at small ϵ. For example, different synchronization regions (Arnold tongues) can overlap, leading to multi-stability. This means that, for certain combinations of f_f and ϵ, periodic oscillations with different rational ratios between the observed and forcing frequencies can coexist. This phenomenon has been experimentally observed by van der Pol & van der Mark (1927) in a low-dimensional oscillator circuit and, as figure 12 shows, is also present in our thermoacoustic system when $f_f/f_n = 1.06$. Figure 12(*a*) shows the familiar quasi-periodic oscillation that arises from a torus-birth bifurcation, followed by lock-in at $\epsilon = 0.12$ via a torus-death bifurcation (not shown). At larger ϵ, the system switches to a periodic oscillation at $f_f/2$ (figure 12*b*). At still larger ϵ, it switches back to the primary synchronization orbit at f_f (figure 12*e*). This occurs because the external forcing modifies the stability of the different attractors, altering their basins of attraction, thus making one state more stable than another depending on ϵ (Pikovsky *et al.* 2003). These results show that besides choosing f_f carefully, in order to maximize the weakening of the self-excited mode, it is also important to examine the stability of the system at lock-in.
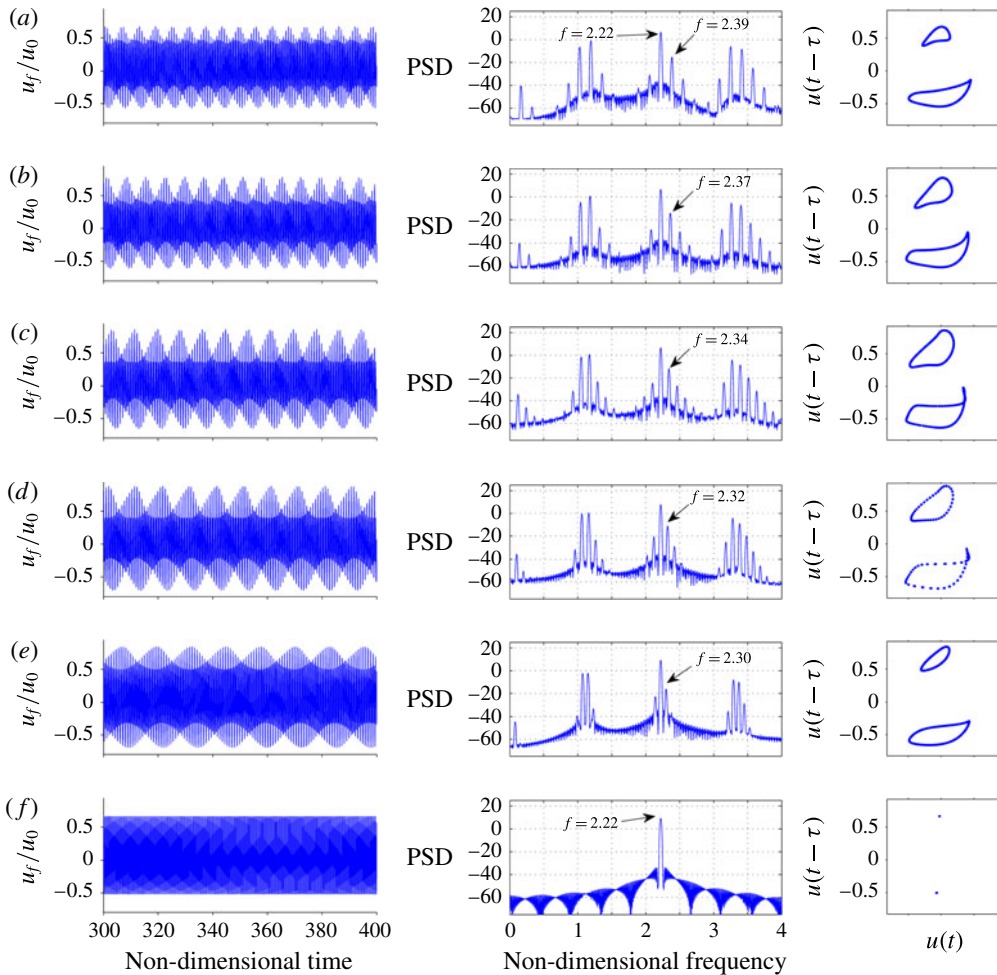
FIGURE 13. (Colour online) Synchronization of a $\mathbb{T}^2$ attractor: the forced response of the system during quasi-periodic oscillations (state C) when forced at the dominant characteristic frequency of its 2-torus, $f_f/f_1 = 1$, where $f_1 = 2.22$. Time series, power spectra and Poincaré maps are shown for increasing forcing amplitudes: (a) $\epsilon \equiv u'_f/U_0 = 0.00$ or unforced, (b) 0.09, (c) 0.18, (d) 0.24, (e) 0.30 and (f) 0.31.

5. Forcing of aperiodic oscillations: states C and D

Kashinath *et al.* (2014) showed that this thermoacoustic system can oscillate not just periodically but also aperiodically. In this section, we examine the forced response of this system when its natural (unforced) self-excited state is quasi-periodic and chaotic.

First we consider the system when it is oscillating quasi-periodically at characteristic frequencies of $f_1 = 2.22$ and $f_2 = 0.17$ (state C in table 1), with the amplitude at f_1 being higher than that at f_2. Figure 13 shows the response of this system when forced at $f_f = f_1$. The time series shows that the beating frequency decreases as ϵ increases. This can be seen in the power spectra as a steady decrease in the bandwidth of the sidebands, indicating frequency pulling. The shape of the 2-torus changes as ϵ increases, until the system undergoes a saddle-node bifurcation to a stable periodic
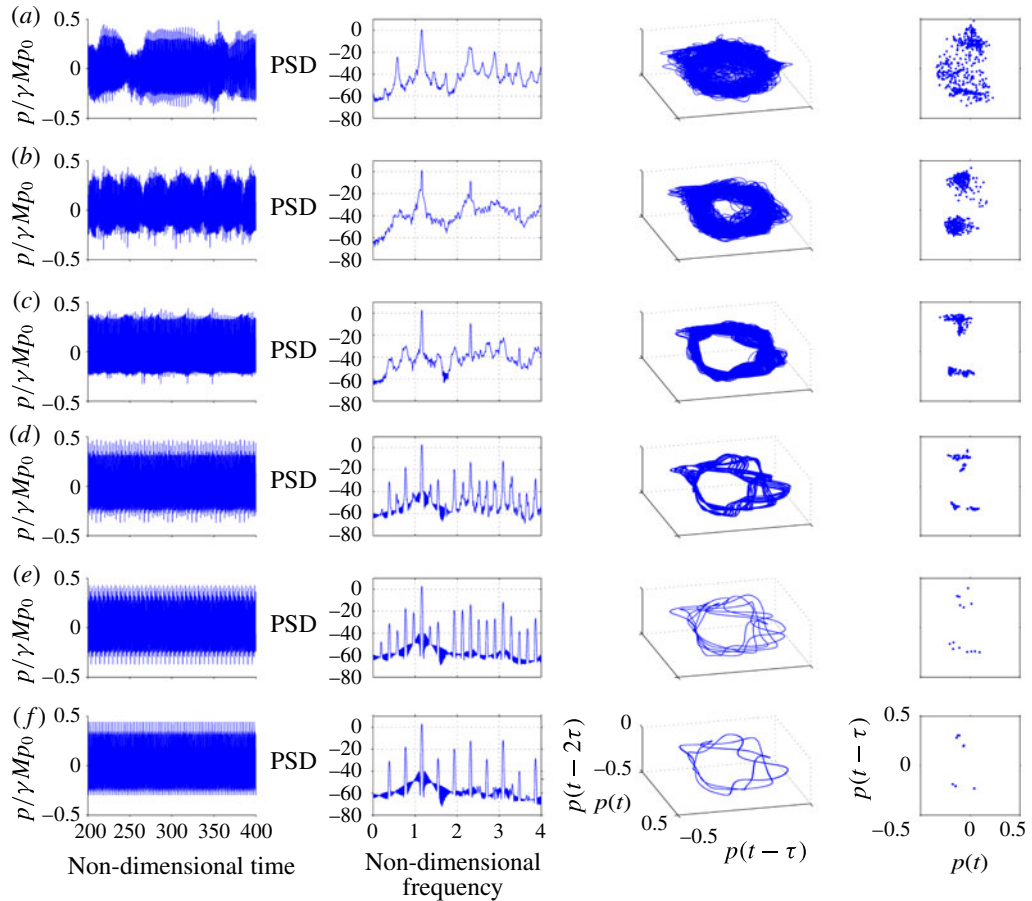
FIGURE 14. (Colour online) Synchronization of a strange attractor: the forced response of the system during chaotic oscillations (state D) when forced at the dominant frequency of its unforced spectrum, $f_f/f_n = 1$, where $f_n = 1.16$. Time series, power spectra, phase portraits and Poincaré maps are shown for increasing forcing amplitudes: (a) $\epsilon \equiv u'_f/U_0 = 0.00$ or unforced, (b) 0.09, (c) 0.18, (d) 0.27, (e) 0.30 and (f) 0.31.

orbit at lock-in (figure 13f). This is the same type of transition and bifurcation as described in §4.1.

Synchronization and control of driven and autonomous chaotic oscillators have been attracting growing interest in the last two decades (Miranda 2004). In particular, the destruction of chaos via lock-in to a stable periodic orbit presents an appealing strategy for open-loop control of chaotic oscillations. The strength of chaos is indicated by the maximal Lyapunov exponent, with stronger chaos requiring stronger forcing to cause chaos destruction. In our previous study (Kashinath *et al.* 2014), we characterized some of the strange attractors associated with chaotic oscillations in this thermoacoustic system by calculating the Lyapunov exponent and the correlation dimension.

Figure 14 shows the response of the system when forced at the dominant frequency of its strange attractor, $f_n = 1.16$ (state D in table 1). As ϵ increases, the time series show the emergence of order, the power spectra show sharper peaks at discrete

frequencies, and the phase portraits and Poincaré maps show a change in the topology of the attractor. With stronger forcing ($\epsilon \sim 0.30$), the system is stabilized to a period-3 orbit (figure 14*e*). Destruction of chaos may be viewed as the stabilization of one of the infinitely many unstable periodic orbits that comprise the strange attractor. When ϵ increases, one (or more) of these unstable periodic orbits is stabilized, resulting in lock-in. One may therefore speculate that the control of chaos could be achieved via a two-step process: (i) stabilize one of the unstable periodic orbits, and then (ii) apply techniques from § 4 to weaken this periodic orbit.

6. Conclusions

We have examined the forced response of a low-order numerical model of a thermoacoustic system consisting of a realistic flame, several acoustic modes and negligible numerical noise. Our aims are: (i) to understand and predict the synchronization behaviour by relating it to that of simple forced nonlinear dynamical systems; (ii) to provide 'clean' test cases against which other numerical or experimental results can be compared; and (iii) to investigate the potential of using open-loop harmonic forcing as a means of weakening self-excited thermoacoustic oscillations that are periodic, quasi-periodic and chaotic.

We find that the forced response of this system is quite elaborate, with the following features. (i) Forced period-1 oscillations have different bifurcations leading up to lock-in, some of which involve transitions to intermittency and chaos. (ii) The critical forcing amplitude required for lock-in depends on two factors: (1) whether the forcing frequency is above or below the natural (self-excited) frequency, and (2) the proximity of the forcing frequency to the natural frequency. (iii) The response amplitude at lock-in may be larger or smaller than that of the unforced system and can exhibit hysteresis (the jump phenomenon) owing to a cusp catastrophe. At certain forcing frequencies, even weak forcing is sufficient to weaken the self-excited oscillations to amplitudes nearly 90 % lower than that of the unforced system. (iv) When the locked-in state is forced at increasing amplitudes, two types of behaviour are observed: (1) the locked-in state loses stability and transitions to chaos via period-doubling bifurcations, or (2) it repeatedly switches between different stable attractors, indicating multi-stability. (v) Finally, quasi-periodic and chaotic oscillations can be synchronized to periodic forcing via different bifurcations, which suggests that weakening an aperiodic oscillation may be possible via a two-step strategy: (1) the aperiodic oscillation is first stabilized to a periodic oscillation by periodic forcing, and then (2) that periodic oscillation is suppressed by additional periodic forcing applied at a frequency far from the frequency of the original forcing. In other words, it may be possible to weaken aperiodic thermoacoustic oscillations via a careful choice of two forcing frequencies and amplitudes, applied sequentially.

In summary, we find that this thermoacoustic system exhibits rich synchronization behaviour, similar to that seen in recent experiments on forced hydrodynamically self-excited jet diffusion flames and low-density jets (Li & Juniper 2013*a*,*b*,*c*) but previously unreported in the literature on thermoacoustics. The numerical model used in this study has around 5000 degrees of freedom and consists of 20 coupled oscillators interacting with each other via a nonlinear heat release rate and perturbed by open-loop harmonic forcing. The behaviour observed in this study, however, suggests that this system behaves similarly to low-dimensional model oscillators. This implies that a low-order dynamical model may exist that is capable of reproducing the dynamics of the larger system. The pursuit of such a model is attractive because

it could provide opportunities to identify the causes of the rich synchronization behaviour, to improve our interpretation of the underlying nonlinear dynamics, and to develop and test new control strategies for weakening self-excited oscillations, as well as making the direct application of well-known results from dynamical systems theory in thermoacoustics possible.

REFERENCES

ABEL, M., AHNERT, K. & BERGWEILER, S. 2009 Synchronization of sound sources. *Phys. Rev. Lett.* **103** (11), 114301.

AFRAIMOVICH, V. S. & SHILNIKOV, L. P. 1983 On invariant two-dimensional tori, their breakdown and stochasticity. In *Methods of the Qualitative Theory of Differential Equations*, pp. 3–26. Gor'kov. Gos. University.

ANNASWAMY, A. M. 2006 Nonlinear modeling and control of combustion dynamics. In *Control of Fluid Flow*, pp. 95–121. Springer.

ARONSON, D. G., ERMENTROUT, G. B. & KOPELL, N. 1990 Amplitude response of coupled oscillators. *Physica* D **41** (3), 403–449.

BALANOV, A., JANSON, N., POSTNOV, D. & SOSNOVTSEVA, O. 2009 1 : 1 forced synchronization of periodic oscillations. In *Synchronization: From Simple to Complex,* chap. 3, Springer.

BALUSAMY, S., LI, L. K. B., HAN, Z., JUNIPER, M. P. & HOCHGREB, S. 2015 Nonlinear dynamics of a self-excited thermoacoustic system subjected to acoustic forcing. *Proc. Combust. Inst.* **35** (3), 3229–3236.

BELAIR, J. & GLASS, L. 1983 Self-similarity in periodically forced oscillators. *Phys. Lett.* A **96** (3), 113–116.

BELLOWS, B. D., HREIZ, A. & LIEUWEN, T. 2008 Nonlinear interactions between forced and self-excited acoustic oscillations in premixed combustor. *J. Propul. Power* **24** (3), 628–631.

BLEVINS, R. D. 1985 The effect of sound on vortex shedding from cylinders. *J. Fluid Mech.* **161**, 217–237.

CHEN, S. C. 1990 Growth and frequency pushing effects in relativistic magnetron phase-locking. *IEEE Trans. Plasma Sci.* **18** (3), 570–576.

DAVITIAN, J., GETSINGER, D., HENDRICKSON, C. & KARAGOZIAN, A. R. 2010 Transition to global instability in transverse-jet shear layers. *J. Fluid Mech.* **661**, 294–315.

DOWLING, A. P. 1997 Nonlinear self-excited oscillations of a ducted flame. *J. Fluid Mech.* **346**, 271–290.

DOWLING, A. P. & MORGANS, A. S. 2005 Feedback control of combustion oscillations. *Annu. Rev. Fluid Mech.* **37**, 151–182.

GABOR, D. 1946 Theory of communication. *J. Inst. Electr. Engrs (London)* **3**, 429–457.

GETSINGER, D. R., HENDRICKSON, C. & KARAGOZIAN, A. R. 2012 Shear layer instabilities in low-density transverse jets. *Exp. Fluids* **53** (3), 783–801.

GIANNAKOPOULOS, K. & DELIYANNIS, T. 2001 Jump phenomenon in an OTA simulated LC circuit. *Intl J. Electronics* **88** (1), 1–11.

GLASS, L., GUEVARA, M. R., BELAIR, J. & SHRIER, A. 1984 Global bifurcations of a periodically forced biological oscillator. *Phys. Lett.* A **29** (3), 1348.

GOTODA, H., AMANO, M., MIYANO, T., IKAWA, T., MAKI, K. & TACHIBANA, S. 2012 Characterization of complexities in combustion instability in a lean premixed gas-turbine model combustor. *Chaos* **22**, 043128.

GOTODA, H., NIKIMOTO, H., MIYANO, T. & TACHIBANA, S. 2011 Dynamic properties of combustion instability in a lean premixed gas-turbine combustor. *Chaos* **21** (1), 013124.

GOTTLIEB, S. & SHU, C. 1998 Total variation diminishing Runge–Kutta schemes. *Math. Comput.* **67** (221), 73–85.

HEMCHANDRA, S. 2009 Dynamics of turbulent premixed flames in acoustic fields. PhD thesis, Georgia Institute of Technology, USA.

HOLMES, P. J. & RAND, D. A. 1978 Bifurcations of the forced van der Pol oscillator. *Q. Appl. Maths* **35**, 495–509.

HOPFIELD, J. J. 1994 Neurons, dynamics and computation. *Phys. Today* **47** (2), 40–46.

HOVEL, P. 2010 *Control of Complex Nonlinear Systems with Delay*. Springer.

HUYGENS, C. 1673 The pendulum clock. In *Horologium Oscillatorium*. Iowa State University Press; translated in 1986.

ILLINGWORTH, S. J. & MORGANS, A. S. 2010 Adaptive feedback control of combustion instability in annular combustors. *Combust. Sci. Technol.* **182** (2), 143–164.

JIANG, G. S. & PENG, D. 2000 Weighted ENO schemes for Hamilton–Jacobi equations. *SIAM J. Sci. Comput.* **21** (6), 2126–2143.

KABIRAJ, L., SAURABH, A., WAHI, P. & SUJITH, R. I. 2012a Route to chaos for combustion instability in ducted laminar premixed flames. *Chaos* **22** (2), 023129.

KABIRAJ, L. & SUJITH, R. I. 2012 Nonlinear self-excited thermoacoustic oscillations: intermittency and flame blowout. *J. Fluid Mech.* **713**, 376–397.

KABIRAJ, L., SUJITH, R. I. & WAHI, P. 2012b Bifurcations of self-excited ducted laminar premixed flames. *Trans. ASME J. Engng Gas Turbines Power* **134** (3), 031502.

KANTZ, H. & SCHREIBER, T. 2003 *Nonlinear Time Series Analysis*, 2nd edn. Cambridge University Press.

KARIMI, N., BREAR, M., JIN, S. H. & MONTY, J. P. 2009 Linear and non-linear forced response of a conical ducted laminar premixed flame. *Combust. Flame* **156** (11), 2201–2212.

KASHINATH, K., WAUGH, I. C. & JUNIPER, M. P. 2014 Nonlinear self-excited thermoacoustic oscillations of a ducted premixed flame: bifurcations and routes to chaos. *J. Fluid Mech.* **761**, 399–430.

LI, L. K. B. 2012 Forcing of globally unstable jets and flames. PhD thesis, University of Cambridge, Department of Engineering, United Kingdom.

LI, L. K. B. & JUNIPER, M. P. 2013a Lock-in and quasiperiodicity in a forced hydrodynamically self-excited jet. *J. Fluid Mech.* **726**, 624–655.

LI, L. K. B. & JUNIPER, M. P. 2013b Lock-in and quasiperiodicity in hydrodynamically self-excited flames: experiments and modelling. *Proc. Combust. Inst.* **34** (1), 947–954.

LI, L. K. B. & JUNIPER, M. P. 2013c Phase trapping and slipping in a forced hydrodynamically self-excited jet. *J. Fluid Mech.* **735** (R5), 1–11.

LIEUWEN, T. C. & YANG, V. 2005 *Combustion Instabilities in Gas Turbine Engines: Operational Experience, Fundamental Mechanisms, and Modeling*. American Institute of Aeronautics and Astronautics.

LUBARSKY, E., SHCHERBIK, D., BIBIK, A. & ZINN, B. T. 2003 Active control of combustion oscillations by non-coherent fuel flow modulation. *AIAA J.* **3180** (9), 730–745.

MIRANDA, J. M. G. 2004 *Synchronization and Control of Chaos: An Introduction for Scientists and Engineers*. Imperial College Press.

NAYFEH, A. H. & BALACHANDRAN, B. 2004 *Applied Nonlinear Dynamics: Analytical, Computational, and Experimental Methods*. Wiley-VCH.

NAYFEH, A. H. & MOOK, D. T. 1995 *Nonlinear Oscillations*. Wiley.

OLINGER, D. J. 1992 Lock-in states in the dripping mode of the capillary jet. *Exp. Fluids* **15** (2), 155–158.

ORCHINI, A., ILLINGWORTH, S. J. & JUNIPER, M. P. 2015 Frequency domain and time domain analysis of thermoacoustic oscillations with wave-based acoustics. *J. Fluid Mech.* **775**, 387–414.

PETROV, V., OUYANG, Q. & SWINNEY, H. L. 1997 Resonant pattern formation in a chemical system. *Nature* **388**, 655–657.

PIKOVSKY, A. S., ROSENBLUM, M. G. & KURTHS, J. 2003 *Synchronization: A Universal Concept in Nonlinear Sciences*. Cambridge University Press.

VAN DER POL, B. 1927 Forced oscillations in a circuit with non-linear resistance. *Phil. Mag.* **3** (13), 65–80.

VAN DER POL, B. & VAN DER MARK, J. 1927 Frequency demultiplication. *Nature* **120** (3019), 363–364.

PREETHAM, SANTOSH, H. & LIEUWEN, T. 2008 Dynamics of laminar premixed flames forced by harmonic velocity disturbances. *J. Propul. Power* **24** (6), 1390–1402.

PROVANSAL, M., MATHIS, C. & BOYER, L. 1987 Bénard–von Kármán instability: transient and forced regimes. *J. Fluid Mech.* **182**, 1–22.

ROMPALA, K., RAND, R. & HOWLAND, H. 2007 Dynamics of three coupled van der Pol oscillators with application to circadian rhythms. *Commun. Nonlinear Sci.* **12** (5), 794–803.

SCHEFFER, M., CARPENTER, S., FOLEY, J. A., FOLKE, C. & WALKER, B. 2001 Catastrophic shifts in ecosystems. *Nature* **413**, 591–596.

SMALL, M. 2005 *Applied Nonlinear Time Series Analysis: Applications in Physics, Physiology and Finance*. World Scientific.

STROGATZ, S. H. 1994 *Nonlinear Dynamics and Chaos*. Perseus Books.

THOMPSON, J. M. T. & STEWART, H. B. 2002 *Nonlinear Dynamics and Chaos*. Wiley.

VENKATESAN, A. & LAKSHMANAN, M. 1997 Bifurcation and chaos in the double-well Duffing–van der Pol oscillator: numerical and analytical studies. *Phys. Rev.* E **56** (6), 6321.

WALSH, J. E., JOHNSTON, G. L., DAVIDSON, R. C. & SULLIVAN, D. J. 1989 Theory of phase-locked regenerative oscillators with nonlinear frequency-shift effects. In *OE/LASE'89*, pp. 161–169. International Society for Optics and Photonics.

WANG, J. & LIM, T. C. 2011 On the boundary between nonlinear jump phenomenon and linear response of hypoid gear dynamics. *Adv. Acoust. Vib.* **2011**, 1–13.

WILLIAMS, F. A. 1994 *Combustion Theory*, 2nd edn. Westview Press.

XIA, M. & SUN, Q. P. 2015 Jump phenomena of rotational angle and temperature of NiTi wire in nonlinear torsional vibration. *Intl J. Solids Struct.* **56–57**, 220–234.